World Conference on
Timber Engineering
Oslo 2023

MONOTONIC TESTS ON BEAM-TO-COLUMN JOINT WITH STEEL LINK FOR TIMBER SEISMIC RESISTANT STRUCTURES

Giacomo Iovane[1], Leonardo Rodrigues[2] , Jorge Branco[3], Beatrice Faggiano[1]

ABSTRACT: For the design of dissipative heavy timber frame structures, in the context of modern seismic design approach based on the mechanical triad of strength, stiffness and ductility, brittle timber failure modes can be avoided by integrating modern timber connection technology into hybrid timber-steel system. The overall seismic performance can be improved, entrusting the dissipation function to ad hoc conceived devices, as an alternative to connections. Steel links located at the ends of the beams are very promising solutions, which can develop plastic hinges, thus providing a ductile behaviour, with a significant dissipative capacity. Besides timber members, as well as connections, to be designed with an adequate over-strength, can remain in elastic field. In this perspective, the paper illustrates the mechanical characterisation through monotonic tests of two different configurations of timber beam-to-column joint with steel link for heavy timber frames, consisting of a timber element connected to a steel link by means of a steel end-plate and glued-in steel rods. The experimental results indicate a satisfactory agreement with the theoretical ones, therefore the suitability of the system and of the design criteria.

KEYWORDS: Seismic resistant timber structures, beam-to-column joints with steel link, monotonic test on joint.

1 INTRODUCTION

Timber material has an elastic and fragile behaviour up to failure, so that, the present anti-seismic regulations, like the European Eurocode 8 [1], indicates that for the seismic design of dissipative timber structures, joints should dissipate a part of the seismic energy through plastic deformations of steel connectors. However, joints are primary structural elements, with a crucial role in bearing the design loads, so that their integrity should be preserved [2]. By integrating modern timber connection technology into hybrid timber-steel system, brittle wood failure modes can be avoided and overall seismic performance improved.

With specific reference to the structural type of Moment Resisting Frames (MRF), recently, some authors have proposed different solutions for dissipative timber structures, by coupling a ductile material like steel to timber [3 - 9].

In particular, Montuori and Sagarese [6] and Montuori [7] have applied to timber beams the steel reduced beam sections, commonly proposed for steel MR frames; as well as Gohlich et al. [10] studied hybrid steel-timber structures, such as buckling restrained braced frame (BRBF) and moment resistant frame (DMRF) with steel links; Yang et al. [11] have delegated the dissipative capacity to a steel box connected to the beam and column by glued bars; Tomasi et al. [8] and Andreolli et al. [9] focused on a beam-column timber joint equipped with steel links for dissipative MR frames.

The paper deals with the latter type of device, such as a timber beam-to-column joint with steel link located at the ends of the beam. It is designed so that the plastic hinge forms in the steel link, achieving a ductile behaviour and a significant dissipative capacity, while timber members and steel connections, having an adequate over-strength as respect to the dissipative links, remains in elastic field. Such connection system, further to an advantageous mechanical performance, has some other interesting properties, like versatility and prefabrication [2, 12, 13].

As regard the design criteria of the study joints, the capacity design method was applied to ensure the collapse hierarchy between the connection subcomponents [12, 13]. The joints behaviour was preliminary studied through numerical analyses, by means of the software ABAQUS FEA [14], in terms of key parameters, like ultimate strength, stiffness, rotation capacity and failure mode [13]. Then the ductile joint system and the proposed design criteria were validated through an experimental campaign carried out in 2019 at the Department of Civil

[1] Beatrice Faggiano, faggiano@unina.it, Giacomo Iovane, giacomo.iovane@unina.it, University of Naples Federico II, Department of Structures for Engineering and Architecture, P.le Tecchio 80, 80125, Naples, Italy;
[2] Leonardo Rodrigues, Leonardo.Rodrigues@nottingham.ac.uk, University of Nottingham, Faculty of Engineering, Nottingham, NG7 2RD, United Kingdom;
[3] Jorge Branco, jbranco@civil.uminho.pt, University of Minho, Department of Civil Engineering, Campus de Azurém 4800-058 Guimarães, Portugal.

https://doi.org/10.52202/069179-0288

Engineering (DECivil) of the University of Minho, in Guimaraes (Portugal), in cooperation with the Department of Structures for Engineering and Architecture of the University of Naples Federico II. 2 monotonic and 2 cyclic tests up to collapse were performed for 2 types of specimen.
In particular, in this work the monotonic tests on the two beam-to-column joints with steel link are presented.

2 SPECIMEN FEATURES AND MANUFACTURING PROCESS

The specimens (Figs. 1, 2a; [13]) are made of a laminated timber beam (GL24h) with a 140x320mm rectangular cross section, 850mm long, equipped at one end with a steel link, HE100A or IPE100 profiles 250mm long (steel grade S355) with two welded end-plates (120x230mm, steel grade S275), with 20mm thickness for the HE100A, 15mm thickness for the IPE100 specimens.

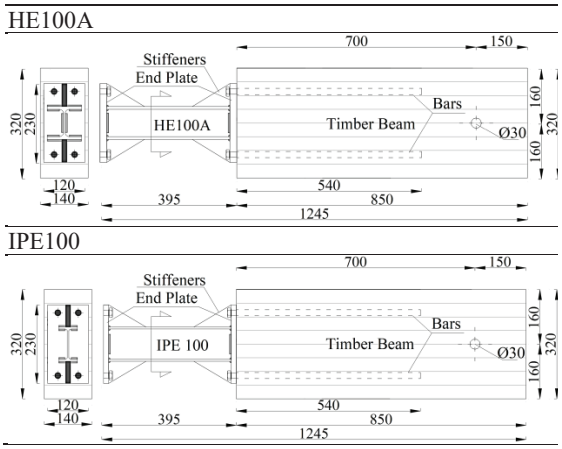

Figure 1: *Specimens geometrical features [mm].*

For both specimens, the link is connected at one side to the timber beam by 4 glued threaded bars (M16, 10.9, 540mm long), at the other side it is rigidly connected to a steel endplate (300x300mm and 40mm thickness) by 4 bolts (M16, 10.9 steel grade, 60mm long). The endplates have four triangular stiffeners (110x67mm for HE100A and 110x65mm for IPE100, with 15mm thickness).
With regards to the insertion of the bars within the timber beam the following manufacturing procedure was applied. On the timber element (Fig. 2b) 4 notches, 49x18mm and 540mm long, were realized guaranteeing an adequate bars anchorage. To ensure the bars centering within the notches, 2mm thick wire was wrapped around each bar, as spacer between bars and internal surface of notches (Fig. 2c). A two-component epoxy resin (Xepox F-liquid, by Rothoblaas) was poured into the notches (Fig. 2d), then the 4 threaded steel bars were inserted. At the end, notches were closed through additional timber elements (31x18mm and 540mm long), previously obtained by the timber rods cut from the timber element for realizing the notches (Fig. 2e, f), ensuring a 18x18mm cavity around the bars. The closing timber elements were sealed using structural timber glue. After gluing, the timber beam was left to dry for 4 days (Fig. 2g).

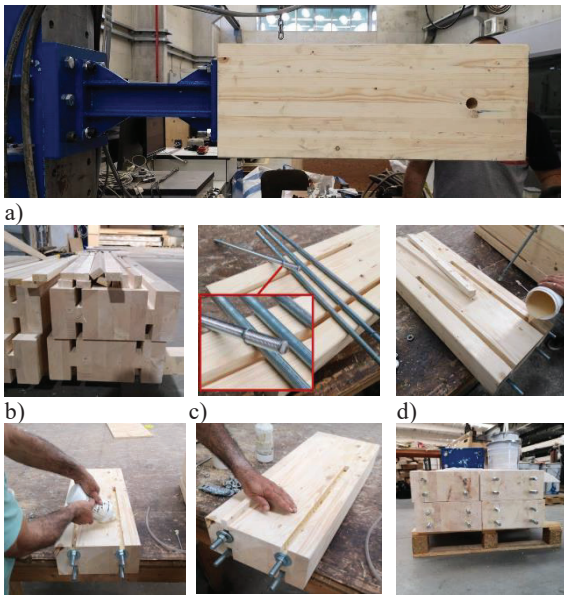

Figure 2: *Manufacturing steps: a) assembled joint; b) notches realization; c) wire spacer around the bars; d) epoxy resin pouring into the notches; e) and f) gluing of additional timber elements; g) timber specimen;.*

3 TEST SET-UP AND EQUIPMENTS

For the tests, a cantilever configuration (Fig. 3a) is realized. At one end, the link is rigidly connected to the reaction steel column of the retaining frame by means of 6 bolts (M12, 10.9 steel grade, 60mm long, Fig. 3b). At the timber beam free-end the load is applied through a pin, inserted in a hole with 30mm diameter drilled at the free-end of the beam. A steel fork connected to the pin ends is used to transfer the load by an hydraulic jack, having a maximum stroke of 200mm (Fig. 3c).

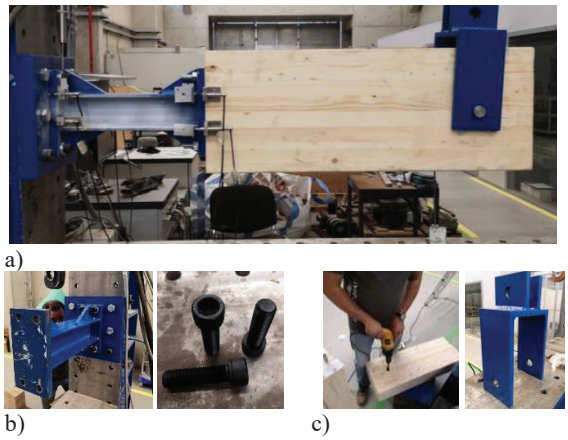

Figure 3: *Test set-up: a) overall set up; details: b) connection of the joint to the retaining frame; c) steel fork.*

The displacements of the specimen during the test are measured by using different types of linear variable displacement transducers (LVDTs). The displacement ranges required to each LVDT were estimated through the preliminary numerical analyses [13]. The LVDTs were installed on the specimen by using aluminium brackets screwed at the timber beam and glued at the steel elements.

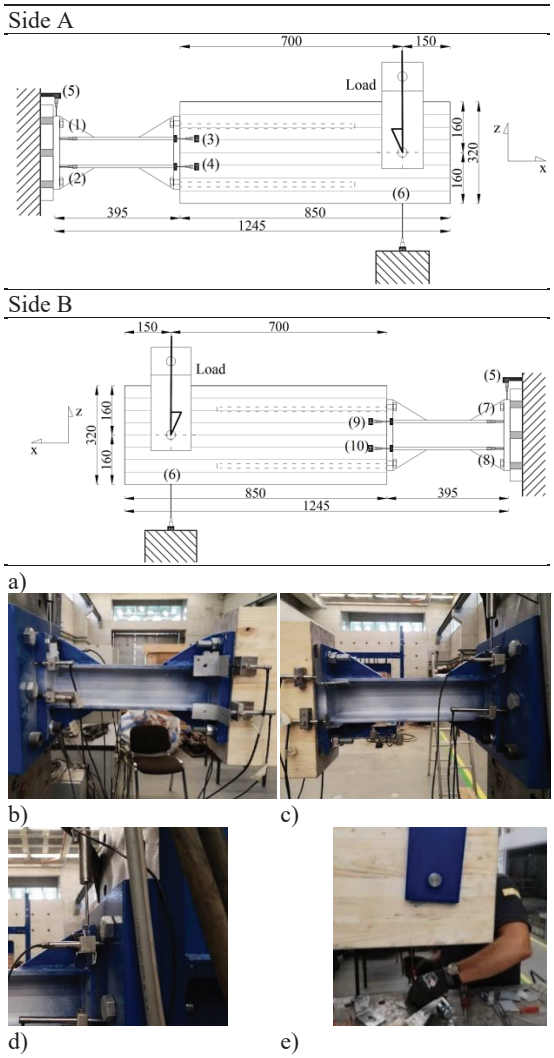

Figure 4: *Displacement transducers position: a) LVDTs on sides A and B [mm]; b) LVDTs nr.1, 2, 3, 4 on side A; c) LVDTs nr.7, 8, 9, 10 on side B; d) LVDT nr.5 at the upper side of the right end-plate; e) LVDT nr.6 at the loading beam section.*

In Figure 4 the position of the LVDTs is shown, they are:

- 4 LVDTs, 2 for each side of the specimens (nr.1 and 2 on side A, Figs. 4a, b; nr. 7 and 8 on side B, Fig. 4a, c) to measure the horizontal displacement between the fixed steel end-plate and the retaining frame;
- 4 LVDTs, 2 for each side of the specimens (nr. 3 and 4 on side A, Fig. 4a, b; nr. 9 and 10 on side B, Fig. 4a, c) to measure the horizontal displacement between the steel link and the timber beam;
- 1 LVDT (nr. 5) placed over the joint end-plate connected to the fixed end-plate to evaluate the possible vertical displacement at the fixed-end of the specimen (Fig. 4a, d);
- 1 LVDT (nr. 6) placed under the hydraulic jack to measure the vertical displacement of the joint at the free-end of the cantilever (Fig. 4a, e).

The LVDTs were calibrated using a large micrometre over a range of ±6 mm. The core of the device is set as close as possible to the zero locations.

The applied force (F) is measured by a load cell (max load: 200kN).

In Figure 5 the overall view of the test set up including the retaining frame is shown.

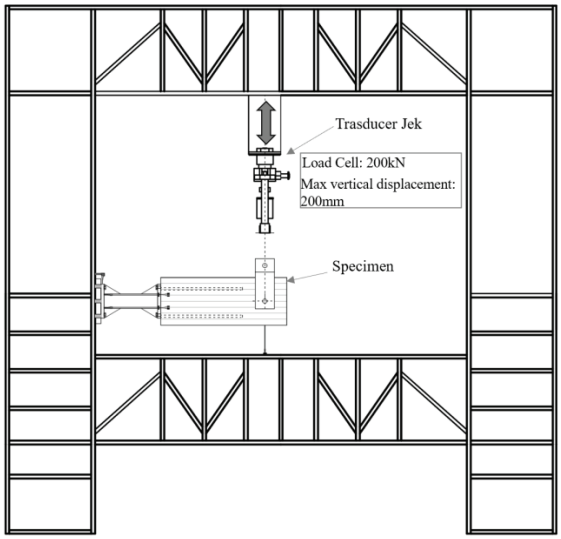

Figure 5: *Overall view of the test set up with the retaining frame.*

4 TEST PROCEDURE AND PERFORMANCE CURVES

The vertical load is applied under displacement control at a constant rate of 0.1mm/s, according to the European standard EN 12512 [15], in order to study the specimen response in elastic-plastic field. Therefore, considering the maximum stroke of the actuator of 200mm, the test end is achieved in about 30 minutes.

The test outputs are provided in terms of force-displacement (F-u) curve. Then, the bending moment-rotation (M-θ) curve is analytically obtained, evaluating the bending moment (M; Eq. 1) and the corresponding rotation (θ; Eq. 2) at the mid-section (M_L point) of the link, according to the following equations (Fig. 6):

$$M = F \cdot L \quad (1)$$

$$\theta = \theta_{Tot} - \theta_A - \theta_B \quad (2)$$

where L is the distance of the mid-section of the link M_L from the load point (L=1020mm); θ_{Tot} is the global rotation of the joint as respect to the retaining frame, θ_A is the rotation of the link left end-plate with respect to the retaining frame, θ_B is the rotation of the link right end-

https://doi.org/10.52202/069179-0288

plate with respect to the timber beam. In particular, the above defined rotations are calculated as it follows with reference to Figure 6:

$$\theta_A = \frac{\delta_{1,7} + \delta_{2,8}}{h_A} \quad (3)$$

$$\theta_B = \frac{\delta_{3,9} + \delta_{4,10}}{h_B} \quad (4)$$

$$\theta_{Tot} = \frac{u_{Tot}}{L_A} \quad (5)$$

where $\delta_{1,7}$ and $\delta_{2,8}$ are the horizontal displacements detected at point A section, evaluated as mean value between the displacements measured with the LVDTs nr. 1, 7 and 2, 8 and h_A is the distance between the LVDTs (Fig. 6b); $\delta_{3,9}$ and $\delta_{4,10}$ are the horizontal x-direction displacements detected at point B section, evaluated as mean value between the displacements measured with the LVDTs nr. 3, 9 and 4, 10 and h_B is the distance between the LVDTs (Fig. 6c); u_{Tot} is the total displacement in vertical z-direction, evaluated at the applied force (F) section by using the LVDT nr. 6 and L_A is the whole length of the joint.

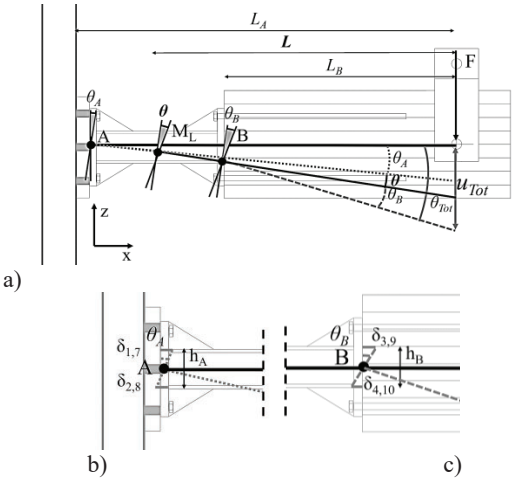

Figure 6: *a) Schematic deformation of the joint and relative rotations between the joint components; b) Rotation between link left end-plate and retaining frame; c) Rotation between link right end-plate and timber beam.*

5 MONOTONIC TEST

In Figure 7, the force-displacement (F-u) curves and the failure modes achieved through the experimental tests are presented. In particular, outputs are noticed at specific selected performance points, defined at the yielding of the steel link (P_Y), the collapse of the specimen (P_C) and a total displacement equal to 200mm (P_{200}), which corresponds to the maximum stroke of the loading actuator.

Both joints show a ductile behaviour with the plastic deformation of the link, achieving the formation of the plastic hinge. HE100A joint reached the maximum stroke of 200mm (coinciding with the end of the test) before the failure (P_C), while IPE100 joint failed (P_C) through the buckling of the link flange, before the achievement of the 200mm total displacement.

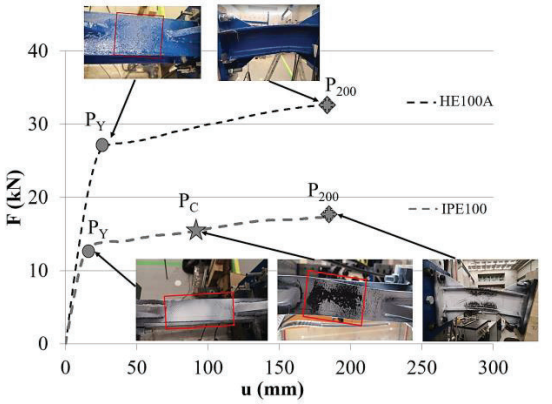

Joint	HE100A		IPE100	
Performance points	**F [kN]**	**u [mm]**	**F [kN]**	**u [mm]**
P_Y	27.11	17.73	12.89	14.96
P_C		-	15.40	97.32
P_{200}	32.71	184.97	17.81	184.97

Figure 7: *Experimental F-u curves of the joints; performance points: Y-yielding, C- collapse, 200-Actuator stroke.*

6 ANALYSIS OF RESULTS

The tests results are discussed in terms of initial stiffness $S_{j,ini}$ (eq. 1), plastic field stiffness $S_{j,pl}$ (eq. 2, 3) and resistance $F_{j,Y}$ at yielding point (P_Y), as well as ductility capacity D_j (eq. 4, 5), evaluated as it follow:

$$S_{j,ini} = \frac{M_{j,el}}{\theta_{j,el}} \quad (1)$$

$$S_{HE100A,pl} = \frac{M_{j,Rd,200}}{\theta_{j,pl,200}} \quad (2)$$

$$S_{IPE100,pl} = \frac{M_{j,Rd,C}}{\theta_{j,pl,C}} \quad (3)$$

$$D_{HE100A} = \frac{u_{200}}{u_Y} \quad (4)$$

$$D_{IPE100} = \frac{u_C}{u_Y} \quad (5)$$

where $M_{j,el}$ and $\theta_{j,el}$ correspond respectively to the elastic bending moment, not exceeding 2/3 $M_{j,Rd}$ ($M_{j,Rd}$ being the design bending strength of the j-joint, [16]), and the rotation at the elastic limit; $M_{j,Rd,C}$ and $\theta_{j,pl,C}$ correspond respectively to the design bending strength and the rotation of the IPE100 at collapse point (P_C); $M_{j,Rd,200}$ and $\theta_{j,pl,200}$ correspond respectively to the design bending strength and the rotation of the HE100A at 200mm vertical displacement (P_{200}); u_{200} is the displacement at P_{200} point, u_C is the displacement at P_C point and u_Y is the displacement at P_Y point.

In particular, HE100A and IPE100 joints performances are compared through the Capacity Ratios (CRs), defined in terms of initial stiffness $S_{j,ini}$ (CR-S_{ini}=$S_{IPE100,ini}$/$S_{HE100A,ini}$), plastic field stiffness $S_{j,pl}$ (CR-S_{pl}=$S_{IPE100,pl}$/$S_{HE100A,pl}$), yielding strength $F_{j,Y}$ (CR-F_Y=$F_{IPE100,Y}$/$F_{HE100A,Y}$) and ductility capacity D_j (CR-

D_j=D_{IPE100}/D_{HE100A}). The mechanical parameters are given in Table 1. Observing the experimental results, IPE100 joint shows lower initial and plastic field stiffnesses, strength and ductility, as respect to HE100A, with CR-S_{ini}=75%, CR-S_{pl}=85%, CR-F_Y=48%, CR-D=75%.

***Table 1**: Joints initial stiffness $S_{j,ini}$, plastic field stiffness $S_{j,pl}$, resistance F_j and ductility capacity D_j for study joints: preliminary numerical and experimental values.*

Joint	**HE100A**		**IPE100**	
Performaces	**Test**	**Num.**	**Test**	**Num.**
$S_{j,ini}$ [kN/rad]	1227	1546	936	1054
$S_{j,pl}$ [kN/rad]	38	16	28	17
$F_{j,Y}$ [kN]	27.11	26.50	12.89	11.61
D_j [-]	10.43	11.48	6.51	7.85

With regards to rotations, it has to be noticed that, in both joints, the maximum θ_B and θ_A rotations are negligible compared to the overall rotation θ_{Tot}, being θ_B/θ_{Tot} equal to 2.2% and 2.3% for HE100A and IPE100 respectively, θ_A/θ_{Tot} equal to 0.5% and 0.7% for HE100A and IPE100 respectively (Tab. 2). This also confirms the efficiency as rigid connections of the link end joints.

***Table 2**: Joints rotations θ_B, θ_A and θ_{Tot} in P_{200} and P_C points respectively for HE100A and IPE100.*

Joint	**HE100A**		**IPE100**	
Points	**P_{200}**		**P_C**	
	[rad]	**θ_i/θ_{Tot}** [%]	[rad]	**θ_i/θ_{Tot}** [%]
θ_B	0.004	2.2	0.002	2.3
θ_A	0.0009	0.5	0.0006	0.7
θ_{Tot}	0.18		0.084	

In Figure 8, the experimental force-displacement (F-u) and the analytically moment-rotation (M-θ) curves are given in comparison with the preliminary numerical ones [13]. In particular, further to the previously defined performance points (P_Y, P_C, P_{200}), on the numerical curve also the point, corresponding to the link full plasticization (P_{PN}), is evidenced.

It is apparent that the experimental and numerical curves are very close in the elastic field, while the post-elastic branches differs. This means that the preliminary model perfectly caught the elastic behaviour, while it has to be calibrated after the laboratory tests. This is also quantified through the Capacity Ratios (CRs) evaluated at the selected performance points (P_i, where i is Y, 200, C), in terms of strength $F_{j,i}$ (CR-$F_{j,i}$=$F_{j,n,i}$/$F_{j,t,i}$), displacement $u_{j,i}$ (CR-$u_{j,i}$=$u_{j,n,i}$/$u_{j,t,i}$), initial stiffness $S_{j,ini}$ (CR-$S_{j,ini}$=$S_{j,n,ini}$/$S_{j,t,ini}$), plastic field stiffness $S_{j,pl}$ (CR-$S_{j,pl}$=$S_{j,n,pl}$/$S_{j,t,pl}$) and ductility capacity D_j (CR-D_j=$D_{j,n}$/$D_{j,t}$; Tab. 3).

With regards to the collapse modes it is worth noticing that the preliminary numerical analysis of HE100A joint reached the failure, beyond the test limit of 200mm (P_{200t}), corresponding to the buckling of the link web (F_{Cn}=29.35kN; u_{Cn}=242mm). Besides the same collapse condition is evidenced for IPE100 in both preliminary numerical analysis and test, corresponding to the buckling of the link flange before P_{200}.

It is not possible to evaluate the collapse hierarchy of the joint sub-components through the experimental tests, however by superimposing the images deriving from the numerical analysis with the photos taken at the end of the test (at P_C for IPE100 and P_{200} for HE100A), a very good approximation of the ultimate deformed configuration of the joints is worth noticed (Fig. 9).

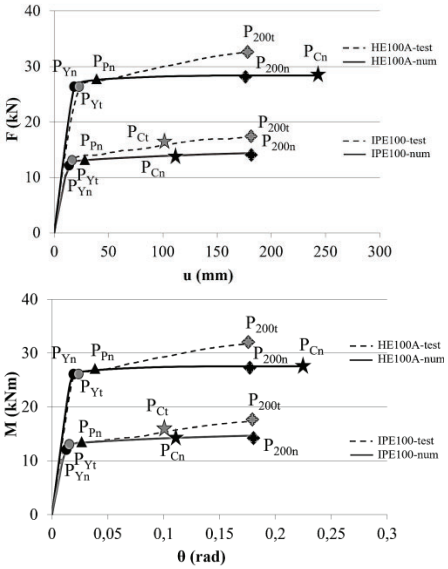

***Figure 8:** Experimental vs preliminary numerical F-u and M-θ curves of the joints; performance points: Y-yielding, C-collapse, 200-Actuator stroke.*

***Table 3**: Joints Capacity Ratios (CRs) in terms $F_{j,i}$, $u_{j,i}$, $S_{j,ini}$, $S_{j,pl}$, and $D_{j,i}$ in P_Y, P_{200} and P_C points for HE100A and IPE100.*

Joint	**HE100A**			**IPE100**		
[%]	**P_Y**	**P_{200}**	**P_C**	**P_Y**	**P_C**	**P_{200}**
Cr-F	98	87	/	90	81	91
Cr-u	98	108	/	89	108	108
CR-S_{ini}	126			114		
Cr-S_{pl}	43			59		
Cr-D	110			121		

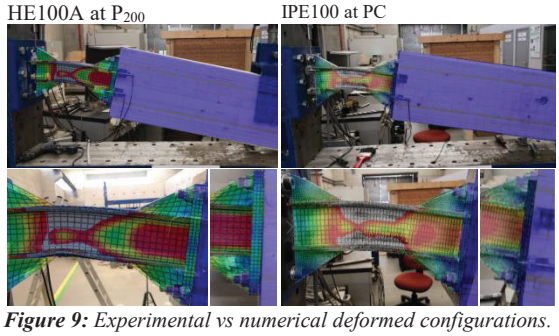

***Figure 9:** Experimental vs numerical deformed configurations.*

7 CONCLUSIVE REMARKS

The paper focuses on beam-to-column joints with dissipative steel link in the timber beam for seismic moment resistant heavy timber framed structures. In

https://doi.org/10.52202/069179-0288

particular, monotonic experimental tests on two joints are presented.

The HE100A and IPE100 joints structural performance was preliminary investigated through monotonic incremental non-linear analyses on refined FE models, examining the key parameters, such as strength, stiffness, rotation capacity and failure modes. Then, the mechanical behaviour of the joints was studied through the capacity curves, F-u and M-θ, obtained through the monotonic tests. The joints performance is evaluated at specific points, corresponding to the link yielding (P_Y), full plasticization of the link (P_P), ultimate strength (P_C) and strength at the actuator stroke equal to 200mm (P_{200}). Results showed that HE100A joint, as respect to IPE100, has higher initial stiffness, plastic field stiffness, strength and ductility. With regards to the collapse conditions, for HE100A joint, the 200mm stroke (P_{200}) occurs before the joint failure, while for IPE100 joint, the failure is achieved before, corresponding to the buckling of the link flange. For HE100A the collapse was attained through the preliminary numerical analysis, corresponding to the buckling of the link web.

Therefore, the experimental results are compared with those of the preliminary numerical analysis. The experimental and numerical curves are coincident in the elastic field, up to the yielding point, while the post-elastic branches are different, evidencing the need to opportunely calibrate the FE models, specially on the basis of the laboratory tests on the materials.

Definitely the tests have validated the theoretical and numerical predictions, confirming the formation of the plastic hinge in the link, which dissipates the energy through plastic deformation, avoiding brittle failures, as well as proving the efficiency of the system and of the proposed design criteria.

The work is in progress toward the development of seismic resistant dissipative timber structures, focusing on the dissipative device design, toward the calibration of the refined numerical model, the extension of both the numerical analyses and test campaigns, to evaluate the cyclic behavior and the dissipation capacity of the beam-to-column joint with steel link. At the same time, the global behavior of seismic resistant timber structure with dissipative links is going to be investigated.

ACKNOWLEDGEMENT

The research project DPC–ReLUIS 2019-2021 and 2022-2024 - WP13 Contribution to standards for timber structures, and the Department of Civil Engineering (DECivil) laboratory of the Minho University, in Guimaraes (Portugal) are acknowledged.

REFERENCES

[1] EN 1998-1: 2004: Eurocode 8: Design of structures for earthquake resistance – Part 1: General rules, seismic actions and rules for buildings (CEN: Comité Européen de Normalisation).

[2] Faggiano B., Iovane G.. First considerations on the design approach and criteria for seismic resistant moment resisting and bracings timber frames. In *World Conf. on Timber Engin.*, 2016. Paper ID1094.

[3] Humbert J., Lee S., Park J., Park M.. Moment resistance of post-and-beam joints with concealed metallic connectors. In *World Conference on Timber Engineering (WCTE)*, 2014.

[4] Komatsu K., Mori T., Kitamori A., Araki Y.. Evaluation on dynamic performance of glulam frame structure composed of slotted bolted connection system. In *World Conference on Timber Engineering*, (WCTE 2014).

[5] Nakatani M., Mori T., Komatsu K.. Performance of semirigid timber frame with Lag screw bolt connections: experimental, analytical, and numerical model results. In *International Journal of Advanced Structural Engineering* 7:387–403, 2015.

[6] Montuori R. and Sagarese V.. The use of steel RBS to increase ductility of wooden beams. In *Engineering Structures.* 169, 154-161. 2018.

[7] Montuori R.. The influence of gravity loads on the seismic design of RBS connections. *The Open Construction and Building Technology Journal*. Betham Open, 8, 248-261, 2014.

[8] Tomasi R., Zandonini R., Piazza M., Andreolli M.. Ductile end connections for glulam beams. In *Structural Engineering International*. 18; 290-296, 2008.

[9] Andreolli M., Piazza M., Tomasi R., Zandonin R.. Ductile moment-resistant steel-timber connections. In Structures and Buildings, 164, SB2, 65-78, 2011.

[10] Gohlich R., Erochko J., Woods J.E.. Experimental testing and numerical modelling of a heavy timber moment-resisting frame with ductile steel links. In *Earthquake Engineering & Structural Dynamics*. 47, 1460-1477, 2018.

[11] Yang H., Wang. C., Hu J., Tao H., Liu J., Tang L., Shi B.. Experimental static and seismic behaviour of glulam beam-to-column connection with screwed-in threaded rod joints. *BioResources* 16(3), 5272-5286, 2021.

[12] Iovane G., Faggiano B., Noviello C., Mazzolani F.M., Landolfo R., Faggiano B.. Beam-to-column joint with steel link for timber structures: system optimization through numerical investigations and design criteria. In *World Conference on Timber Engineering (WCTE),* 2020

[13] Iovane G., Faggiano B.. Timber beam-to-column joint with steel link: design and mechanical characterization through numerical investigation. *8th Int. Conference on Computational Methods in Structural Dynamics and Earthquake Engineering* (COMPDYN), vol. 1, 2359-2365, 2021.

[14] ABAQUS FEA 2022 - Abaqus/CAE, or “Complete Abaqus Environment”.

[15] EN 12512: 2001/A1: 2005: Timber Structures - Test methods - Cyclic testing of joints made with mechanical fasteners (CEN, French: Comité Européen de Normalisation).

[16] EN 1993: 2005: Eurocode 3: Design of steel structures. Part 1-8: Design of joints (CEN: Comité Européen de Normalisation).